






# Regulation of the Mitochondrion-Fatty Acid Axis for the Metabolic Reprogramming of *Chlamydia trachomatis* during Treatment with $\beta$ -Lactam Antimicrobials

 Kensuke Shima,<sup>a</sup> Inga Kaufhold,<sup>a</sup> Thomas Eder,<sup>b,c</sup> Nadja Käding,<sup>a</sup> Nis Schmidt,<sup>a</sup> Iretiolu M. Ogunsulire,<sup>a</sup> René Deenen,<sup>d</sup> Karl Köhrer,<sup>d</sup>  Dirk Friedrich,<sup>a</sup> Sophie E. Isay,<sup>a</sup> Florian Grebien,<sup>c</sup> Matthias Klinger,<sup>e</sup> Barbara C. Richer,<sup>f</sup> Ulrich L. Günther,<sup>f</sup> George S. Deepe, Jr.,<sup>g</sup> Thomas Rattei,<sup>b</sup>  Jan Rupp<sup>a,h</sup>

<sup>a</sup>Department of Infectious Diseases and Microbiology, University of Lübeck, Lübeck, Germany

<sup>b</sup>Division of Computational Systems Biology, University Vienna, Vienna, Austria

<sup>c</sup>Institute for Medical Biochemistry, University of Veterinary Medicine Vienna, Vienna, Austria

<sup>d</sup>Biological and Medical Research Center (BMFZ), Heinrich Heine University Düsseldorf, Düsseldorf, Germany

<sup>e</sup>Institute of Anatomy, University of Lübeck, Lübeck, Germany

<sup>f</sup>Institute of Chemistry and Metabolomics, University of Lübeck, Lübeck, Germany

<sup>g</sup>Division of Infectious Diseases, College of Medicine, University of Cincinnati, Cincinnati, Ohio, USA

<sup>h</sup>German Center for Infection Research (DZIF), Partner Site Hamburg-Lübeck-Borstel-Riems, Lübeck, Germany

**ABSTRACT** Infection with the obligate intracellular bacterium *Chlamydia trachomatis* is the most common bacterial sexually transmitted disease worldwide. Since no vaccine is available to date, antimicrobial therapy is the only alternative in *C. trachomatis* infection. However, changes in chlamydial replicative activity and the occurrence of chlamydial persistence caused by diverse stimuli have been proven to impair treatment effectiveness. Here, we report the mechanism for *C. trachomatis* regulating host signaling processes and mitochondrial function, which can be used for chlamydial metabolic reprogramming during treatment with  $\beta$ -lactam antimicrobials. Activation of signal transducer and activator of transcription 3 (STAT3) is a well-known host response in various bacterial and viral infections. In *C. trachomatis* infection, inactivation of STAT3 by host protein tyrosine phosphatases increased mitochondrial respiration in both the absence and presence of  $\beta$ -lactam antimicrobials. However, during treatment with  $\beta$ -lactam antimicrobials, *C. trachomatis* increased the production of citrate as well as the activity of host ATP-citrate lyase involved in fatty acid synthesis. Concomitantly, chlamydial metabolism switched from the tricarboxylic acid cycle to fatty acid synthesis. This metabolic switch was a unique response in treatment with  $\beta$ -lactam antimicrobials and was not observed in gamma interferon (IFN- $\gamma$ )-induced persistent infection. Inhibition of fatty acid synthesis was able to attenuate  $\beta$ -lactam-induced chlamydial persistence. Our findings highlight the importance of the mitochondrion-fatty acid interplay for the metabolic reprogramming of *C. trachomatis* during treatment with  $\beta$ -lactam antimicrobials.

**IMPORTANCE** The mitochondrion generates most of the ATP in eukaryotic cells, and its activity is used for controlling the intracellular growth of *Chlamydia trachomatis*. Furthermore, mitochondrial activity is tightly connected to host fatty acid synthesis that is indispensable for chlamydial membrane biogenesis. Phospholipids, which are composed of fatty acids, are the central components of the bacterial membrane and play a crucial role in the protection against antimicrobials. Chlamydial persistence that is induced by various stimuli is clinically relevant. While one of the well-recognized inducers,  $\beta$ -lactam antimicrobials, has been used to characterize chlamydial persistence, little is known about the role of mitochondria in persistent infection. Here, we demonstrate how *C. trachomatis* undergoes metabolic reprogramming to switch from

**Citation** Shima K, Kaufhold I, Eder T, Käding N, Schmidt N, Ogunsulire IM, Deenen R, Köhrer K, Friedrich D, Isay SE, Grebien F, Klinger M, Richer BC, Günther UL, Deepe GS, Jr, Rattei T, Rupp J. 2021. Regulation of the mitochondrion-fatty acid axis for the metabolic reprogramming of *Chlamydia trachomatis* during treatment with  $\beta$ -lactam antimicrobials. *mBio* 12:e00023-21. <https://doi.org/10.1128/mBio.00023-21>.

**Editor** Scot P. Ouellette, University of Nebraska Medical Center

**Copyright** © 2021 Shima et al. This is an open-access article distributed under the terms of the [Creative Commons Attribution 4.0 International license](https://creativecommons.org/licenses/by/4.0/).

Address correspondence to Kensuke Shima, [kensuke.shima@uksh.de](mailto:kensuke.shima@uksh.de).

**Received** 8 January 2021

**Accepted** 23 February 2021

**Published** 30 March 2021

the tricarboxylic acid cycle to fatty acid synthesis with promoted host mitochondrial activity in response to treatment with  $\beta$ -lactam antimicrobials.

**KEYWORDS** *Chlamydia trachomatis*, citrate, STAT3, beta-lactams, fatty acids, metabolism, mitochondria, penicillin, persistence, protein tyrosine phosphatase

Each year, more than 130 million people are infected with the obligate intracellular bacterium *Chlamydia trachomatis* worldwide (1). Infections induce inflammatory tissue damage in the upper genital tract that is linked to severe sequelae such as pelvic inflammatory disease (PID) and infertility in women (1).

Productive *C. trachomatis* exhibits a unique biphasic life cycle that alternates between two morphological forms, infectious elementary bodies (EBs) and replicating reticulate bodies (RBs) (2). However, the chlamydial persistent form containing aberrant RBs is induced by several stimuli such as  $\beta$ -lactams or gamma interferon (IFN- $\gamma$ ) (3–10). While penicillin is known for one of the best-characterized *in vitro* chlamydial persistence models (3, 7, 11–13), amoxicillin is clinically considered an alternative therapeutic drug for *C. trachomatis* in pregnant women (14, 15). Although amoxicillin is not a front-line antimicrobial against *C. trachomatis* infection,  $\beta$ -lactams are commonly prescribed for various bacterial infections in the United States (16) and for the treatment of different bacterial sexually transmitted diseases (STDs) (3–7, 14). Acute infection with *C. trachomatis* is often asymptomatic (15). Therefore, amoxicillin that may be used to treat a urinary tract infection, for example, might induce persistence in patients who are asymptotically infected with *C. trachomatis* (7). Importantly, it has been reported that the efficacy of first-line antimicrobials such as doxycycline and azithromycin against the persistent phenotype of *C. trachomatis* is reduced (3, 17).  $\beta$ -Lactams have also been used to uncover chlamydial basic medical science such as the mechanism of cell division (18–20).

Although *C. trachomatis* is able to generate its own ATP, mitochondrial activity and various mitochondrion-derived metabolites are essentially needed for its intracellular development (2, 10, 21). Genome sequencing revealed that *C. trachomatis* lacks many metabolic genes (22), including several genes in the chlamydial tricarboxylic acid (TCA) cycle (23). Therefore, *C. trachomatis* has to hijack host mitochondrion-derived 2-oxoglutarate and glutamine that is further catabolized to glutamate and 2-oxoglutarate in order to initiate the chlamydial TCA cycle (22–24).

Mitochondrion-derived citrate is an essential metabolite for the synthesis of host fatty acids (25). It is also known that *C. trachomatis* depends on host-derived lipids for its life cycle (26–31). Although *C. trachomatis* carries genes for fatty acid and chlamydial membrane synthesis, the pathogen lacks some genes that play a key role in the synthesis of unsaturated fatty acids (22, 26–28). Consequently, *C. trachomatis* utilizes host-derived fatty acids and lipids for its own membrane biogenesis to compensate for the truncated chlamydial lipid metabolic pathway (26–28, 32).

One of the regulators of mitochondrial activity is signal transducer and activator of transcription 3 (STAT3) (33–37). Tyrosine phosphorylation of STAT3 at position 705 (STAT3 pY<sup>705</sup>) is important to form active STAT3 that downregulates mitochondrial activity in primary mouse embryonic fibroblasts (34–36). Active STAT3 not only reduces mitochondrial membrane potential but also diminishes protein levels of representative components of the electron transport chain (ETC), especially complexes IV and V (34, 36). Hence, this downregulation further leads to reductions in respiratory chain activity and mitochondrial ATP production (34, 36). Furthermore, it is known that serine phosphorylation of STAT3 at position 727 (STAT3 pS<sup>727</sup>) localizes in mitochondria and enhances mitochondrial functions (37). While STAT3 is phosphorylated at position 705 during various cytokine receptor signaling events, including interleukin-6 (IL-6), it is negatively regulated by seven different phosphotyrosine phosphatases (PTPs) (38). Furthermore, negative regulation occurs by suppressor of cytokine signaling 3 (SOCS3) and protein inhibitor of activated STAT (PIAS) (39).

Although host mitochondrial activity is crucial for the life cycle of *C. trachomatis*, little is known about how *C. trachomatis* subverts host signaling processes and utilizes mitochondrial functions in chlamydial persistence.

In this study, we show a unique response that chlamydial metabolism switched from the TCA cycle to fatty acid synthesis in  $\beta$ -lactam-induced chlamydial persistence, which is linked to PTP-STAT3-regulated mitochondrial activity.

## RESULTS

**Mitochondrial activity is enhanced in productive *C. trachomatis* infection.** To investigate mitochondrial responses in *C. trachomatis* infection, we first measured mitochondrial respiration in the absence of antimicrobials. Mitochondrial activity as defined by basal respiration, ATP-linked respiration, and maximal respiration was increased in *C. trachomatis*-infected cells compared to noninfected control cells at 24 h postinfection (hpi) (Fig. 1A). In accordance with the upregulation of mitochondrial activity, the complex IV and V proteins MT-CO1 (mitochondrially encoded cytochrome oxidase I) and ATP5A1 (ATP synthase, H<sup>+</sup> transporting, mitochondrial F1 complex, alpha subunit 1, cardiac muscle) in the ETC were upregulated in *C. trachomatis*-infected cells at 24 hpi (see Fig. S1A and B in the supplemental material). Furthermore, chlamydial growth was inhibited when cells were treated with a mitochondrial ETC complex III inhibitor, antimycin A (Fig. S1C).

Mitochondrial activity is both positively and negatively regulated by STAT3 (33, 34, 37). However, nothing is known about this regulation in *C. trachomatis* infection as of now. Therefore, we analyzed the phosphorylation level of STAT3. *C. trachomatis* infection strongly reduced STAT3 pY<sup>705</sup> but not STAT3 pS<sup>727</sup> at 24 hpi (Fig. 1B and Fig. S1D). To gain insight into the mechanism of reduced STAT3 pY<sup>705</sup>, we investigated the expression levels of SOCS3 and PTPs. Although STAT3 pY<sup>705</sup> was reduced in *C. trachomatis*-infected cells at 24 hpi, there was no difference in SOCS3 protein amounts between *C. trachomatis*-infected cells and noninfected control cells (Fig. S1E). On the other hand, PTPN2, PTPN9, and PTPRK were significantly upregulated in *C. trachomatis*-infected cells compared to noninfected cells at 24 hpi (Fig. S1F). By inhibiting the PTPs using sodium orthovanadate, the effect of *C. trachomatis* infection on STAT3 pY<sup>705</sup> expression was blocked (Fig. S1G).

To elucidate the role of STAT3 phosphorylation in host mitochondrial activity as well as chlamydial replication, we silenced STAT3 using RNA interference (RNAi) (small interfering RNA [siRNA]) (Fig. S1H and J). Inhibition of STAT3 had no impact on the overall infection rates of *C. trachomatis* (Fig. S1L). However, mitochondrial respiration was increased following knockdown of STAT3 in *C. trachomatis*-infected cells at 24 hpi compared to control cells (Fig. S1N). Concomitant with this finding, infectious progeny was increased following the knockdown of STAT3 (Fig. S1P). Similar results were obtained using another siRNA targeting a different sequence of STAT3 (Fig. S1I, K, M, O, and Q). These results indicate that STAT3 functions as a regulator of mitochondrial activity in *C. trachomatis* infection, thereby controlling infectious progeny of *C. trachomatis*.

**Regulation of STAT3 and mitochondrial activity in *C. trachomatis*-infected cells during treatment with  $\beta$ -lactam antimicrobials.** We next assessed whether the observed regulation of PTPs-STAT3 and mitochondrial respiration was altered during treatment with  $\beta$ -lactam antimicrobials. Transmission electron microscopy (TEM) and/or immunofluorescence staining revealed chlamydial persistent morphology indicated by aberrant RBs in penicillin or a therapeutically relevant serum concentration (7) of amoxicillin (Fig. S2A to C). Aberrant RBs are known to be in a viable but noncultivable state, and they can reenter the productive developmental cycle when  $\beta$ -lactam antimicrobials are removed (7). Accordingly, a decrease in infectious progeny was observed in penicillin- or amoxicillin-treated cells, and aberrant RBs were reactivated by the removal of  $\beta$ -lactam antimicrobials (Fig. S2D to F).

During penicillin treatment, basal respiration, ATP-linked respiration, and maximal respiration were elevated, as seen in productive infection at 24 hpi (Fig. 1A). In line

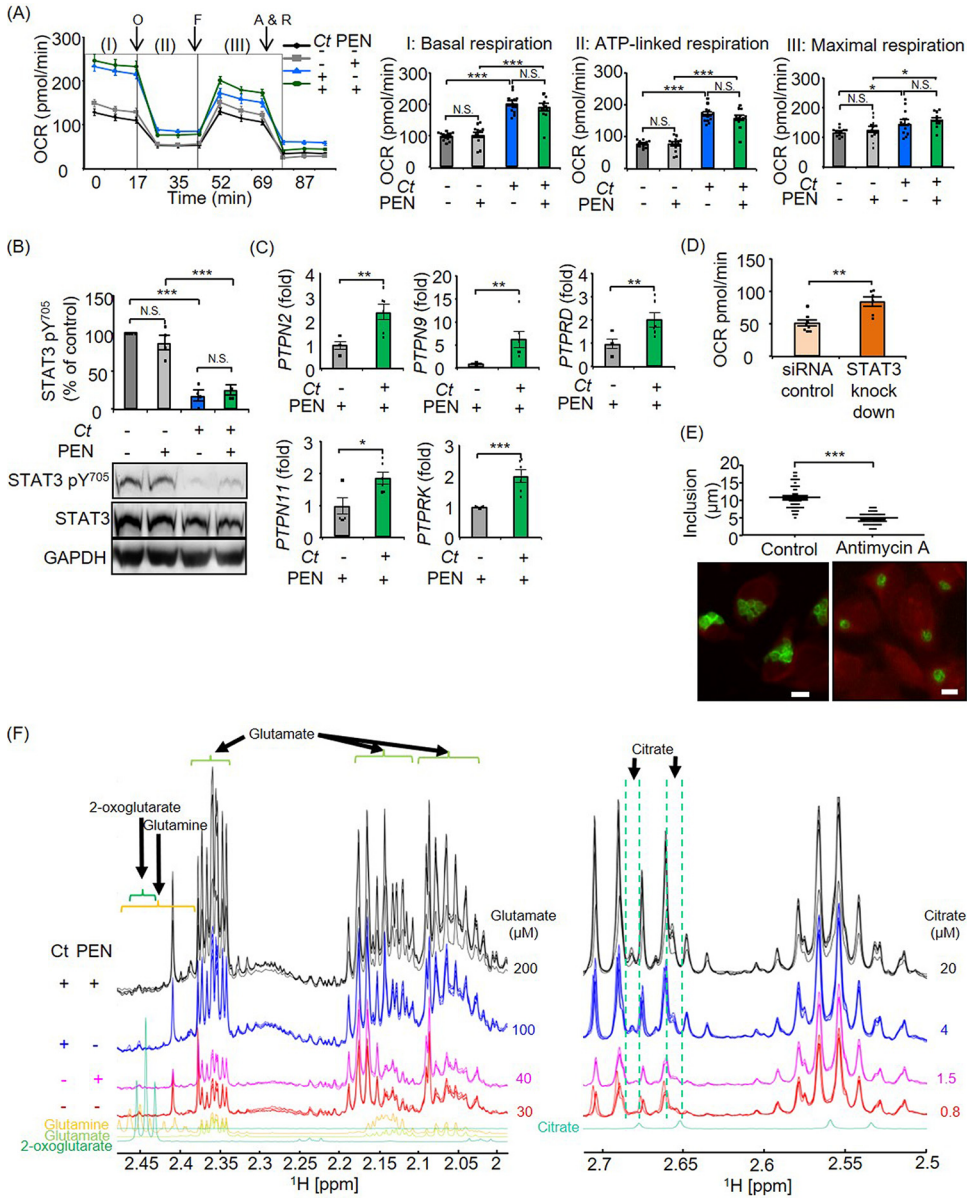


**FIG 1** Analysis of mitochondrial activities and STAT3 regulation in productive and penicillin (PEN)-induced chlamydial persistence. (A) Mitochondrial activity was measured by using a Mito stress test kit at 24 hpi. OCR, oxygen consumption rate; O, oligomycin; F, carbonyl cyanide-4-(trifluoromethoxy)phenylhydrazone (FCCP); A & R, antimycin A plus rotenone. I, II, and III indicate basal respiration, ATP-linked respiration, and maximal respiration, respectively. (B) STAT3 pY<sup>705</sup> in productive and penicillin-induced chlamydial persistence was analyzed by Western blot and densitometric analyses at 24 hpi. STAT3 pY<sup>705</sup> was normalized to total STAT3 proteins. (C) Expression of PTPs in penicillin-induced chlamydial persistence was analyzed by qRT-PCR at 24 hpi. (D) Maximal respiration of siRNA control cells and STAT3 knockdown cells (STAT3HSS186130) in penicillin-induced chlamydial persistence. (E) Size of inclusions and representative images of penicillin-induced chlamydial persistence in 0.2 μM antimycin A-treated and nontreated cells at 24 hpi. Bars = 10 μm. (F) Section of <sup>1</sup>H-NMR spectra expanded between 2 and 2.45 ppm and between 2.5 and 2.7 ppm of deproteinized extracts of control cells (red lines), penicillin-treated cells (magenta lines), *C. trachomatis* (Ct)-infected cells (blue lines), and *C. trachomatis*-infected cells in the presence of penicillin (black lines). Signals arising from each of these metabolites are marked. Deconvolution of overlapping signals was achieved using Chenomx software. Glutamate and citrate concentrations are shown on the right side of each line ( $n = 12$  to  $14$  from four independent experiments [A],  $n = 4$  [B],  $n = 6$  [C],  $n = 6$  to  $8$  from two independent experiments [D],  $n = 57$  to  $77$  [E], and  $n = 3$  to  $5$  [F]) (means ± SEM) (\*,  $P \leq 0.05$ ; \*\*,  $P \leq 0.01$ ; \*\*\*,  $P \leq 0.001$ ; N.S., not significant [by Sidak's multiple-comparison test {A and B} and Student's  $t$  test {C to E}]).

with this result, STAT3 pY<sup>705</sup> was reduced, similar to the observation in productive infection at 24 hpi (Fig. 1B). Concordant with the downregulation of STAT3 pY<sup>705</sup>, not only PTPN2, PTPN9, and PTPRK but also PTPN11 and PTPRD were upregulated by penicillin treatment at 24 hpi (Fig. 1C). To elucidate the link between reduced STAT3 pY<sup>705</sup> and enhanced mitochondrial activity in penicillin-induced chlamydial persistence, we inhibited STAT3 using siRNA (Fig. S1H and J). In penicillin-induced chlamydial persistence, mitochondrial respiration was increased in STAT3 knockdown cells compared to control cells at 24 hpi (Fig. 1D). Accordingly, the formation of enlarged RBs and chlamydial inclusions was inhibited when the mitochondrial ETC was blocked by antimycin A at 24 hpi (Fig. 1E).

Since *C. trachomatis* needs mitochondrion-derived metabolites for its intracellular survival, we performed a targeted analysis of the 2-oxoglutarate family, including glutamine, glutamate, and 2-oxoglutarate, as well as citrate using nuclear magnetic resonance (NMR) spectroscopy. Each of these metabolites can be detected in NMR spectra of cell extracts by simulating the signals of each spin system using Chenomx software. This software also allows one to calculate the concentration of the metabolite based on signal intensities compared to the deuterated TMSP [3-(trimethylsilyl)-2,2,3,3-tetra-deuteriopropionic acid] reference. This analysis revealed that glutamate, which can be catabolized to 2-oxoglutarate, was increased in *C. trachomatis* infection compared to control cells, and this elevation was not suppressed by penicillin treatment at 24 hpi (Fig. 1F). Moreover, we detected a 5-fold higher concentration of citrate in penicillin-induced persistent infection than in productive infection (Fig. 1F).

We showed a similar trend of PTP-STAT3 regulation and mitochondrial activation in amoxicillin treatment at 24 hpi (Fig. S3A to C), indicating that mitochondrial activity plays a pivotal role not only in productive infection but also in penicillin- and amoxicillin-induced chlamydial persistence.

**Fluorescence lifetime imaging microscopy of reduced NAD(P)H in productive *C. trachomatis* and penicillin-induced chlamydial persistence.** Mitochondrial respiration was activated in both productive and  $\beta$ -lactam-induced persistent infection. Thus, we next investigated the chlamydial metabolism that could be linked to mitochondrial activity in productive and persistent infection. Fluorescence lifetime imaging microscopy (FLIM) of NAD(P)H has been demonstrated as a suitable tool for real-time analysis of chlamydial metabolism in living cells (10, 40). Chlamydial metabolism was comparable between productive and penicillin-induced persistent infection at 24 hpi (Fig. 2A and B). In productive infection, however, the fluorescence lifetime of protein-bound NAD(P)H [ $\tau_2$ -NAD(P)H] values inside the chlamydial inclusions were reduced at 36 hpi compared to those at 24 hpi (Fig. 2A and B). This finding indicates an increase in metabolically less active EBs at 36 hpi (Fig. 2C), whereas  $\tau_2$ -NAD(P)H did not change in aberrant RBs induced by penicillin at between 24 and 36 hpi, suggesting that aberrant RBs remain metabolically active over a longer period (Fig. 2A and B).

**Interconnection of host mitochondrial activity and differentially expressed chlamydial metabolic genes in  $\beta$ -lactam-induced chlamydial persistence.** NAD(P)H detected by FLIM might originate from the oxidative pentose phosphate pathway (PPP) or other energy-rich metabolic pathways, including the TCA cycle, of *C. trachomatis* (40). However, it is still unclear where NAD(P)H is generated from and how host mitochondrial activity is utilized by  $\beta$ -lactam-induced persistent *C. trachomatis*. Therefore, we subsequently performed chlamydial transcriptome analysis to identify which chlamydial metabolic pathways are up- or downregulated in penicillin treatment at 24 hpi.

Chlamydial growth curve and TEM analyses revealed that 24 hpi is the mid-log phase of the RB-to-EB transition in productive infection (Fig. S2A and Fig. S4A). When we analyzed gene expression in penicillin-induced persistence compared to productive *C. trachomatis*, the substrate-specific porin PorB (*porB*) as well as chlamydial TCA cycle-related genes were downregulated in penicillin-induced persistent infection (Fig. 3 and Table S1). Flagellar-type ATPases were downregulated in penicillin-induced persistent infection (Fig. 3 and Table S1). Chlamydial glucose-6-phosphate (G-6-P) isomerase (*pgi*),



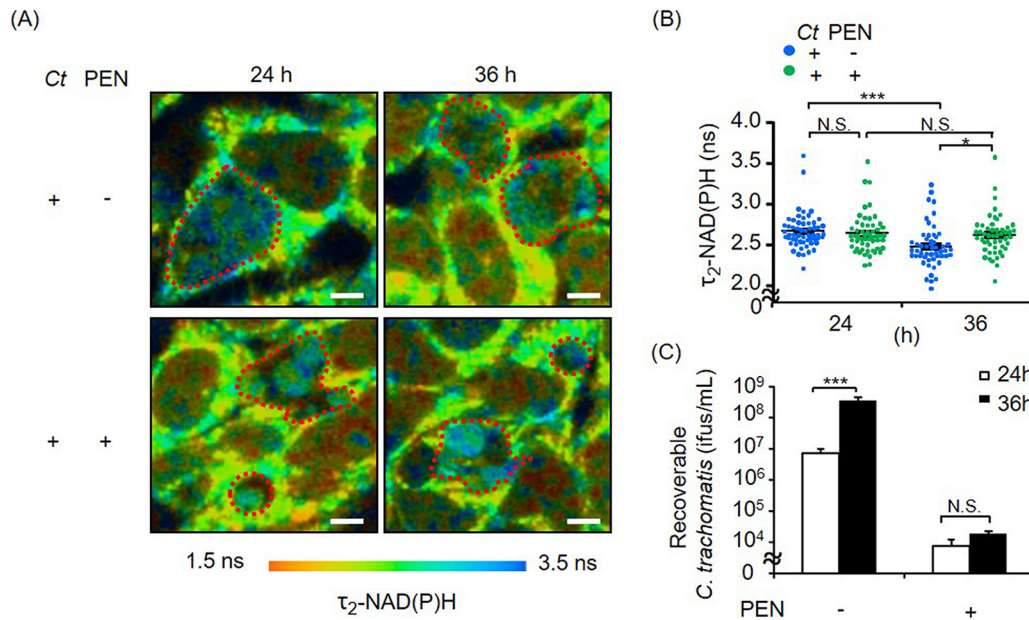


**FIG 2** FLIM of NAD(P)H in productive *C. trachomatis* (Ct) and penicillin (PEN)-induced chlamydial persistence.  $\tau_2$ -NAD(P)H in chlamydial inclusions was analyzed by two-photon microscopy. This enabled real-time imaging of chlamydial metabolic changes. (A and B) Color-coded images of  $\tau_2$ -NAD(P)H (A) and the corresponding quantitative analysis (B) of chlamydial inclusions. Inside the red dots are chlamydial inclusions. Bars = 10  $\mu$ m. (C) Numbers of EBs shown by recovery assays at 24 and 36 hpi. ( $n=51$  to 57 from three independent experiments [A and B] and  $n=3$  to 4 [C]) (means  $\pm$  SEM) (\*,  $P \leq 0.05$ ; \*\*\*,  $P \leq 0.001$ ; N.S., not significant [by Sidak's multiple-comparison test]).

which is the key enzyme to catalyze G-6-P to fructose-6-phosphate, was also downregulated in penicillin-induced persistent infection (Fig. 3 and Table S1), whereas the rate-limiting enzyme G-6-P dehydrogenase (*zwf*) in the chlamydial PPP was upregulated in penicillin-induced persistent infection, indicating that G-6-P could be mainly used for the chlamydial oxidative PPP but not for glycolysis in penicillin-induced persistent infection (Fig. 3 and Table S1). In addition, chlamydial acetyl-CoA production and fatty acid synthesis-associated genes, including enoyl-acyl carrier protein reductase (*fabI*) and V-ATPase, were upregulated in penicillin-induced chlamydial persistence (Fig. 3 and Table S1).

To validate transcriptome analysis in penicillin-induced persistent infection, a subset of chlamydial TCA cycle and other metabolism-related genes were also analyzed by quantitative real-time PCR (qRT-PCR) at 24 hpi. Thus, we could confirm the correlation of gene expressions between RNA sequencing (RNA-seq) and quantitative PCR (qPCR) data (Fig. S4B). We also confirmed a similar trend of expression patterns in a subset of metabolic genes during amoxicillin-induced persistent infection at 24 hpi (Fig. S4C).

In the analysis of RNA-seq, some of the differentially expressed genes in fatty acid biosynthesis were changed  $<2$ -fold between productive and penicillin-induced persistent infection. Therefore, we investigated whether these differences are biologically relevant. To examine the correlation between gene expression and chlamydial fatty acid/phospholipid synthesis, we inhibited chlamydial *FabI*, which is required for the synthesis of fatty acids, influencing the permeability of various molecules and the functions of membrane proteins. While subinhibitory concentrations of 0.4 or 0.6  $\mu$ M *FabI* inhibitor (AFN-1252) did not attenuate inclusion formation in productive infection, the same concentrations of the inhibitor significantly reduced the sizes of inclusions and aberrant RBs in penicillin-induced chlamydial persistence, indicating the biological relevance of differentially expressed fatty acid biosynthetic genes in penicillin-induced persistence (Fig. 4A to C).

**Comparison of differentially expressed chlamydial metabolic genes between  $\beta$ -lactam- and IFN- $\gamma$ -induced chlamydial persistence.** In persistence models, IFN- $\gamma$ -induced chlamydial persistence is clinically relevant (9, 41–44). In our previous study, we showed that IFN- $\gamma$  significantly reduced *C. trachomatis*-induced upregulation of mitochondrial

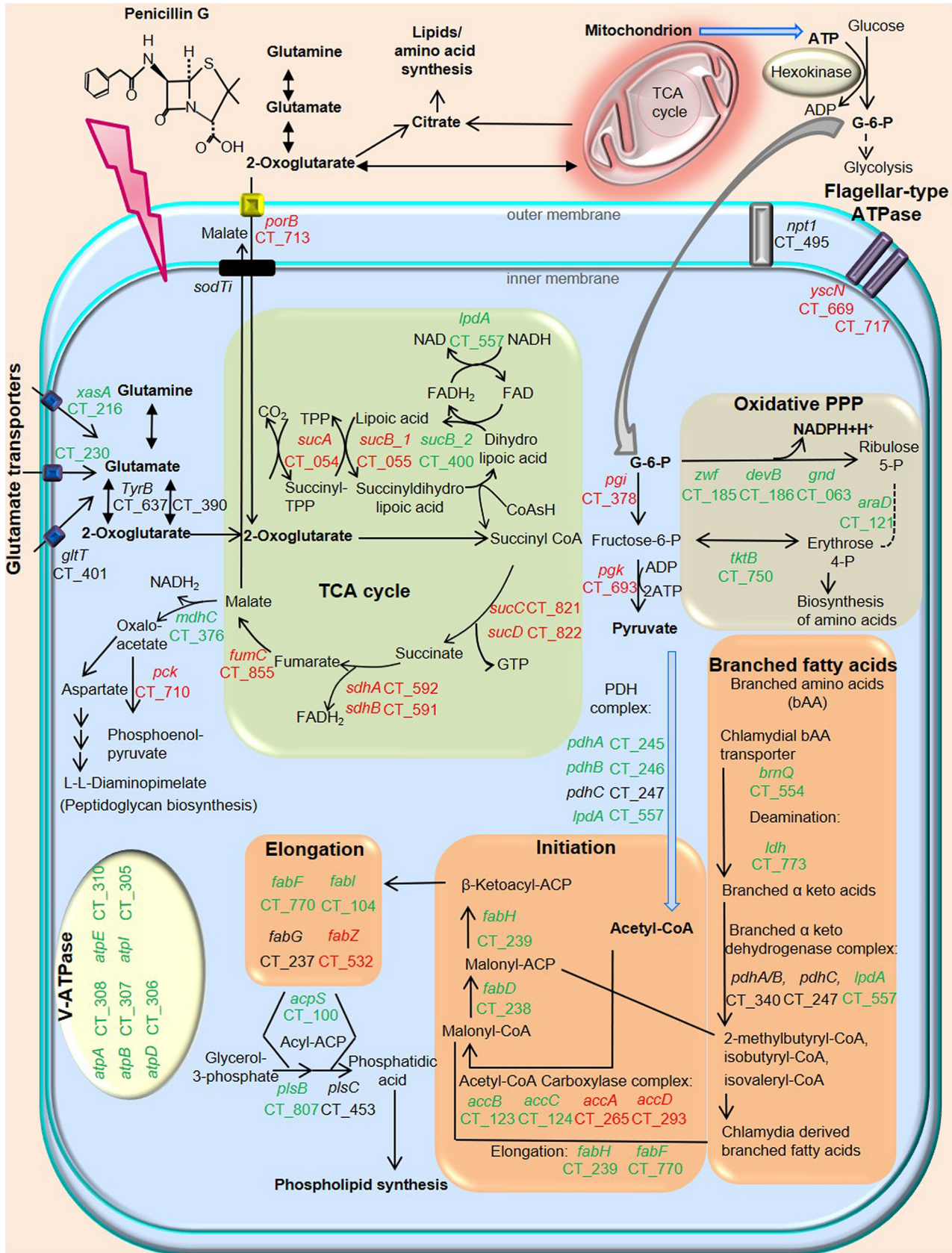


**FIG 3** Schematic representation of the metabolic pathways of *C. trachomatis* during treatment with penicillin. Genes marked in green were significantly upregulated, while genes marked in red were downregulated, in penicillin-induced chlamydial persistence compared to productive (Continued on next page)

respiration. Thus, this cytokine influences mitochondrial respiration differently than that observed with penicillin-induced persistence (10). Since chlamydial metabolism is strongly influenced by host metabolic activity, we investigated whether the expression pattern of chlamydial metabolic genes also differs in IFN- $\gamma$ -induced chlamydial persistence.

In line with a previous report (9), we observed persistent morphology and a massive upregulation of the *trpRBA* operon, which was consistent with the deprivation of host L-tryptophan, as well as *euo*, which functions as a regulator of late gene expression in IFN- $\gamma$ -induced persistent infection compared to productive infection (Table S2 and Fig. S5A) (9). When we analyzed the gene expression patterns of penicillin- and IFN- $\gamma$ -induced persistent *C. trachomatis*, only 26% and 38% of up- or downregulated genes were correlated between the two persistent infections, signifying diverse gene expression patterns (Fig. S5B and C). While we showed the upregulation of fatty acid biosynthesis-related genes in  $\beta$ -lactam-induced persistent infection compared to productive infection, this result was not observed in IFN- $\gamma$ -induced persistent infection (Tables S1 and S2). An interesting similarity is that both inducers cause downregulation of chlamydial TCA cycle-related gene expression (Fig. S5D).

**Impact of host cell fatty acid metabolism on penicillin-induced chlamydial persistence.** Since continued mitochondrial respiration is a unique response in  $\beta$ -lactam-induced persistent infection, we further investigated the role of mitochondria in  $\beta$ -lactam-induced persistent infection. Citrate can be exported from the mitochondrial TCA cycle to the cytosol and becomes a substrate for fatty acid synthesis (25, 45). We showed a higher concentration of citrate in penicillin-induced persistent infection, in accordance with increased host mitochondrial respiration (Fig. 1A and F). Therefore, we determined whether ATP-citrate lyase (ACL), the primary enzyme responsible for the synthesis of acetyl-CoA from citrate for fatty acid synthesis, is activated during penicillin treatment.

Although the protein amount of ACL was not altered, higher catabolic activity of ACL shown by the level of ACL pS<sup>455</sup> was observed in penicillin-treated cultures at 24 hpi (Fig. 4D). Significant increases in other fatty acid metabolism-associated enzymes such as cytoplasmic acetyl-CoA synthase (AceCS1) and mammalian long-chain acyl-CoA synthetase (ACSL1) were detected during penicillin treatment (Fig. 4E and F). Since higher catabolic activity of ACL was observed in penicillin treatment, we investigated the impact of host fatty acid synthesis on the size of aberrant RBs and inclusion formation in penicillin-induced chlamydial persistence. The fatty acid synthase inhibitor C75 significantly attenuated the sizes of aberrant RBs and inclusions in penicillin-induced chlamydial persistence (Fig. 4G). Furthermore, this inhibitor reduced the number of aberrant RBs in each inclusion, indicating a block of the residual division of aberrant RBs. While we cannot totally exclude the possibility that some of the observed effects of C75 could be due to the inhibition of chlamydial fatty acid synthesis, bacterial and human fatty acid synthases share very little sequence homology (46). Therefore, we argue that activated host mitochondria play a key role in ATP production as well as in the supply of citrate to synthesize host fatty acids, which can be utilized in chlamydial persistence during treatment with  $\beta$ -lactam antimicrobials.

## DISCUSSION

Mitochondria play a pivotal role in different cellular processes such as ATP generation, fatty acid synthesis, redox balance, as well as Ca<sup>2+</sup> homeostasis (47). It is known

### FIG 3 Legend (Continued)

infection ( $P_{\text{adj}} \leq 0.05$ ). Chlamydial energy production-associated genes are downregulated in penicillin-induced chlamydial persistence. The chlamydial substrate-specific porin PorB (*porB*), TCA cycle-related genes, and flagellar-type ATPase are downregulated in penicillin-induced chlamydial persistence. Hexokinase of mammalian cells requires mitochondrial ATP to catalyze the conversion of glucose into G-6-P, an essential substrate for chlamydial glycolysis. While chlamydial G-6-P isomerase (*pgi*) is downregulated, the rate-limiting enzyme G-6-P dehydrogenase (*zwf*) in the chlamydial PPP is upregulated in penicillin-induced chlamydial persistence, indicating that G-6-P could be mainly used for the chlamydial PPP. Furthermore, chlamydial fatty acid/phospholipid synthesis as well as acetyl-CoA synthesis are upregulated in penicillin-induced chlamydial persistence. This upregulation is linked to chlamydial phospholipid synthesis. Both acetyl-CoA and oxidative PPP-derived specific NADPH are essential for fatty acid synthesis. FAD, flavin adenine dinucleotide; FADH<sub>2</sub>, reduced flavin adenine dinucleotide; ACP, acyl carrier protein; CoA, coenzyme A.



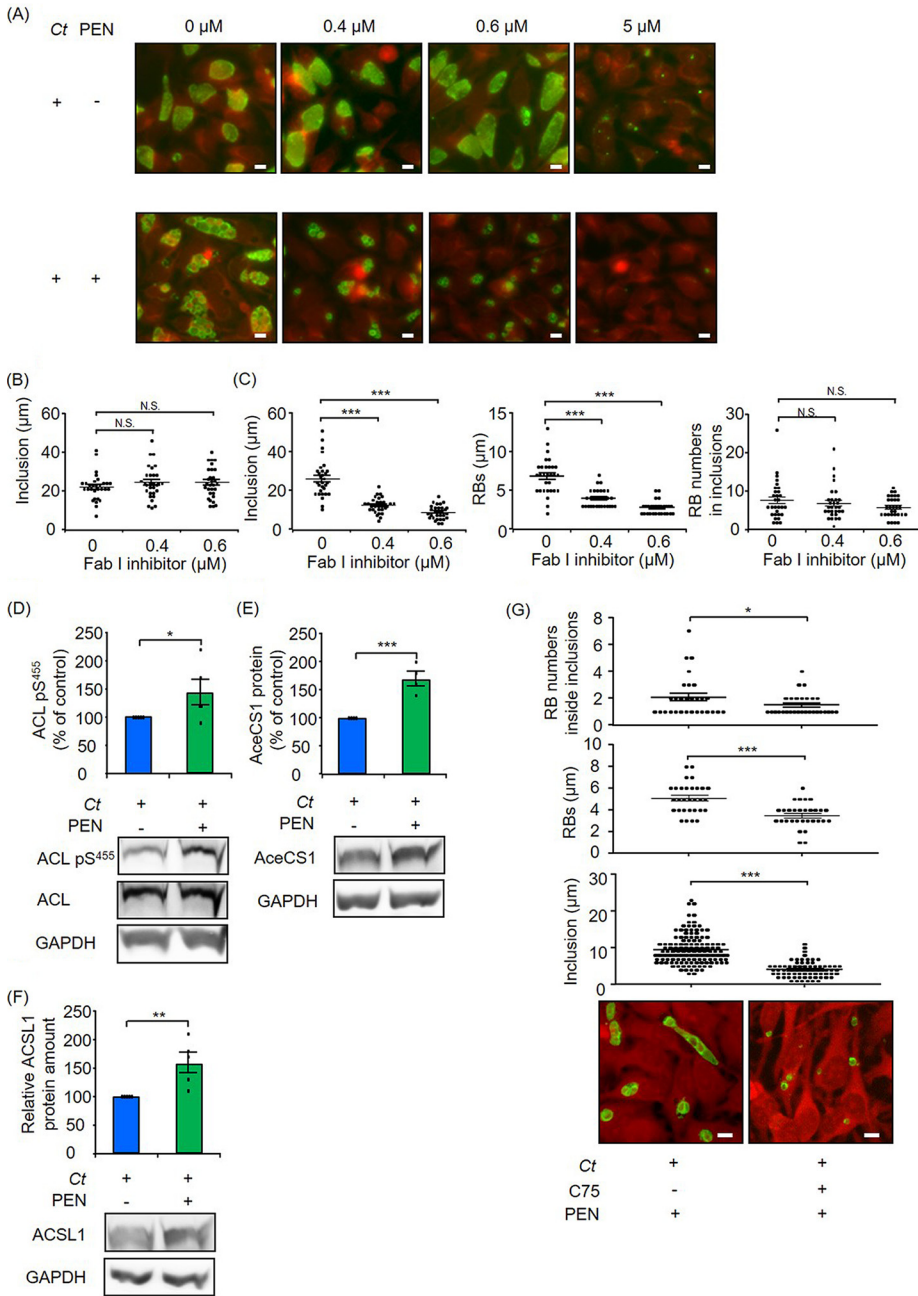


**FIG 4** Role of host-pathogen fatty acid synthesis in penicillin (PEN)-induced chlamydial persistence. (A to C) Effect of the bacterial FabI inhibitor. (A) Representative images of productive and penicillin-induced persistent infection in the presence or absence of the FabI inhibitor AFN-1252 at 24 hpi. Green, immunofluorescence staining with FITC-labeled monoclonal chlamydial LOS antibodies; red, Evans blue counterstaining of host cells. Bars = 10  $\mu$ m. (B) Size of chlamydial inclusions with or without AFN-1252 in productive infection at 24 hpi. (C) Sizes of chlamydial inclusions and aberrant RBs as well as numbers of aberrant RBs inside inclusions with or without AFN-1252 in penicillin-induced chlamydial persistence at 24 hpi. (D to G) Impact of host fatty acid metabolism on penicillin-induced chlamydial persistence. ACL pS<sup>455</sup> (D) as well as AceCS1 (E) and ACSL1 (F) protein amounts were analyzed by Western blot and densitometric analyses at 24 hpi. ACL pS<sup>455</sup> was normalized to total ACL, and AceCS1 and ACSL1 protein amounts were normalized to GAPDH. (G) Representative images of penicillin-induced persistent infection in the presence or absence of the host fatty acid synthetic inhibitor C75 at 24 hpi. Green, immunofluorescence staining with FITC-labeled monoclonal chlamydial LOS antibodies; red, Evans blue counterstaining of host cells. Bars = 10  $\mu$ m. The sizes of chlamydial inclusions and aberrant RBs as well as the numbers of aberrant RBs inside inclusions were analyzed in the presence or absence of C75. *Ct*, *C. trachomatis* ( $n = 30$  from three independent experiments [B and C];  $n = 5$  [D];  $n = 4$  [E];  $n = 5$  [F]; and  $n = 72$  to 140 for the size of inclusions,  $n = 31$  for the size of aberrant RBs, and  $n = 29$  for aberrant RB numbers inside inclusions, from three independent experiments [G]) (means  $\pm$  SEM) (\*,  $P \leq 0.05$ ; \*\*,  $P \leq 0.01$ ; \*\*\*,  $P \leq 0.001$ ; N.S., not significant [by Sidak's multiple-comparison test {B and C} and Student's *t* test {D to G}]).

that various kinds of proteins such as STAT3, mitochondrial transcription factor A (TFAM), mitofusin (MFN), and dynamin-related protein 1 (DRP1) are associated with biogenesis, fusion, and fission of mitochondria (21, 34, 47). In this study, we demonstrated a chlamydial metabolic switch that is linked to PTP-STAT3 pY<sup>705</sup>-regulated mitochondrial activity in  $\beta$ -lactam-induced persistent infection.

Activation of STAT3 is a common host immune response caused by not only various bacteria such as *Salmonella enterica* serovar Typhimurium, *Mycobacterium tuberculosis*, and *Helicobacter pylori* (48–50) but also viruses, including hepatitis B, hepatitis C, herpes, and human immunodeficiency viruses (51). In contrast, here, we demonstrated that *C. trachomatis* causes inactivation of STAT3, which is observed in limited viral infections such as severe acute respiratory syndrome (SARS) coronavirus and human papillomavirus type 6 or type 11 (51–53). Importantly, similar PTP-STAT3 regulation was also observed in *C. trachomatis*-infected primary cells (see Fig. S1R to S1T in the supplemental material).

The protein tyrosine kinases activate STAT3, while PTPs play a key role in hydrolyzing the phosphotyrosine of STAT3. In total, 81 PTPs are active in human cells (54), of which 7 PTPs have been shown to inactivate STAT3 (38). In our study, we showed that mitochondrial activity was significantly enhanced by the inactivation of STAT3 in *C. trachomatis* infection.

In host cells, 2-oxoglutarate is an important intermediate in the mitochondrial TCA cycle, and glutamine is one of the important carbon sources to be catabolized to 2-oxoglutarate (22–24). The first process of glutamine metabolism involves its conversion to glutamate by the mitochondrial matrix-localized phosphate-dependent glutaminase (55). Glutamate is further catabolized to 2-oxoglutarate, which can be used in the mitochondrial TCA cycle. In *C. trachomatis* infection, glutamine is rapidly utilized via glutaminolysis and the TCA cycle in order to generate glutamate and other metabolites such as 2-oxoglutarate (24). Since citrate synthase, aconitate hydratase, and isocitrate dehydrogenase are lacking in the chlamydial TCA cycle (22, 23), *C. trachomatis* has to acquire host cell-derived 2-oxoglutarate using the porin PorB or glutamine/glutamate that can be catabolized to 2-oxoglutarate to fuel its own TCA cycle (23, 24, 56). Therefore, we suggest that mitochondrial activation via PTPs-STAT3 plays a key role in the generation of ATP as well as the enhancement of glutamine metabolism to compensate for the truncated chlamydial TCA cycle in productive *C. trachomatis* infection.

Chlamydial persistence is induced under treatment with  $\beta$ -lactam antimicrobials (3–7). In line with a previous study (7), we observed aberrant RBs during treatment with penicillin and amoxicillin. Importantly, this phenotype can also activate mitochondria concordant with increased PTPs and reduced STAT3 pY<sup>705</sup>. Since  $\beta$ -lactam antimicrobial treatment could not attenuate host mitochondrial activity, we speculated that bacterial metabolic activity is also sustained under  $\beta$ -lactam antimicrobial treatment. In previous studies, we demonstrated that changes in the fluorescence lifetime of  $\tau_2$ -NAD(P)H inside the chlamydial inclusion indicate chlamydial metabolic activity (10, 40). NAD(P)H binds to at least 334 known proteins such as lactate dehydrogenase (LDH) and pyruvate dehydrogenase (PDH) (57). This interaction causes different NAD(P)H fluorescence lifetimes, which are linked to diverse physiological functions (40, 58). Although inclusion morphology is altered in productive and penicillin-induced chlamydial persistence, we documented that chlamydial metabolic activities as defined by the fluorescence lifetime of  $\tau_2$ -NAD(P)H were similar in both chlamydial forms at the mid-log phase but not the late log phase of the organism's developmental cycle.

Because NAD(P)H is generated by different metabolic pathways, we analyzed gene expression using transcriptome analysis and qPCR. To perform this assay, we selected a mid-log phase of the RB-to-EB transition at 24 hpi (Fig. S4A) since we assumed that aberrant RBs are induced from RBs in the developmental cycle. While we morphologically observed a large number of RBs in productive infection at 24 hpi (Fig. S2A), expression of late genes that function in RB-to-EB differentiation was observed at 24 hpi (9, 59). Therefore, we are aware that the interpretation of the observed changes in gene expression could be influenced by the stage of chlamydial development.

In  $\beta$ -lactam-induced chlamydial persistence, PorB (*porB*) and chlamydial TCA cycle-

related genes were downregulated compared to productive *C. trachomatis* at 24 hpi. This downregulation was already observed at 18 hpi before the RB-to-EB transition (Fig. S4A and D). However, the transcriptome analysis revealed that the expression levels of *npt1* (Ct\_495) encoding the chlamydial ATP/ADP translocase are similar between productive and penicillin-induced chlamydial persistence ( $\log_2$  fold change of  $-0.2$ ; adjusted  $P$  value [ $P_{\text{adj}}$ ] of 0.06), and V-ATPases were upregulated in penicillin-induced chlamydial persistence. Although it remains to be experimentally proven whether V-ATPase functions as an ATP synthase, these gene expressions might be involved in the acquisition and production of ATP in penicillin-induced chlamydial persistence (22, 60).

Interestingly, fatty acid synthesis as well as oxidative PPP and acetyl-CoA synthesis were upregulated in  $\beta$ -lactam-induced chlamydial persistence compared to productive *C. trachomatis*. This activation of metabolic pathways is in line with the mechanism of fatty acid synthesis in mammalian cells. NADPH derived from the oxidative PPP as well as acetyl-CoA is essential for fatty acid synthesis (61). As we hypothesized that fatty acid synthesis plays a key role in chlamydial persistence, we could show that the expression of *FabI* had a stronger impact on chlamydial persistence than productive *C. trachomatis*. Since the *FabI* inhibitor does not induce persistence, we suggest that blocking fatty acid synthesis could be an effective treatment for general chlamydial infection.

Since *C. trachomatis* lacks some genes for fatty acid synthesis, it has to hijack host-derived fatty acids and lipids for chlamydial membrane biogenesis (26–28). In host cells, citrate is exported from the mitochondrial TCA cycle to the cytosol and becomes a substrate for host fatty acid synthesis (25), which is catalyzed by ATP-dependent ACL. Furthermore, reductive glutamine metabolism involves the conversion of 2-oxoglutarate to citrate, which is used as a carbon source to fuel fatty acid synthesis (62). In fact, we observed a higher concentration of citrate and increased catabolic activity of ACL shown by the level of ACL pS<sup>455</sup> in penicillin treatment at 24 hpi. Besides, we confirmed the higher protein levels of host *AceCS1* and *ACSL1*, which function to produce acetyl-CoA in penicillin-treated cells.

While  $\beta$ -lactam antimicrobials cause dysregulation of peptidoglycan organization and cell division (18–20, 63), IFN- $\gamma$  depletes tryptophan via the induction of the enzyme indoleamine 2,3-dioxygenase, resulting in the formation of aberrant RBs (41–44). Transcriptome analysis revealed very little overlap of differentially expressed genes between  $\beta$ -lactam- and IFN- $\gamma$ -induced persistence. While 632 genes were differentially expressed in penicillin-induced persistence, only 357 genes were up- or downregulated in IFN- $\gamma$ -induced persistence (Fig. S5B and C). Since a large number of differentially expressed transcription-associated genes were also detected in penicillin-induced persistent infection and IFN- $\gamma$ -induced persistence, this finding highlights the differences in gene expression in the two persistence models.

For reactivation assays, reports show that IFN- $\gamma$ -induced chlamydial aberrant RBs were reversible and that nearly 100% of aberrant RBs were reactivated after the removal of IFN- $\gamma$  (9, 17). On the other hand, our results show that the levels of reactivated *C. trachomatis* in penicillin- and amoxicillin-induced persistence were approximately 3 logs and 1 log lower than in the untreated control, respectively. In line with a previous study (9), our transcriptome analysis revealed that the expression levels of cell division-associated genes, including *CT\_739*, are similar between productive infection and IFN- $\gamma$ -induced persistence ( $\log_2$  fold change of  $-0.19$ ;  $P_{\text{adj}}$  of 0.7). However, this expression was significantly suppressed in penicillin-induced persistence (Table S1). Therefore, we suggest that stress induced by  $\beta$ -lactams exerts a stronger impact on reactivation than IFN- $\gamma$ .

Finally, plasmids are known as a chlamydial virulence factor and impact persistence *in vivo* in a mouse model (64–67). Since we observed that plasmid replication- and maintenance-associated genes were significantly upregulated in both penicillin- and IFN- $\gamma$ -induced persistence compared to productive infection, their functional relevance and impact on mitochondrial and chlamydial metabolism have to be further elucidated.

In conclusion, the regulation of PTPs-STAT3 and ACL activity leads to an enhancement of the mitochondrion-fatty acid synthetic axis; thereby, *C. trachomatis* can

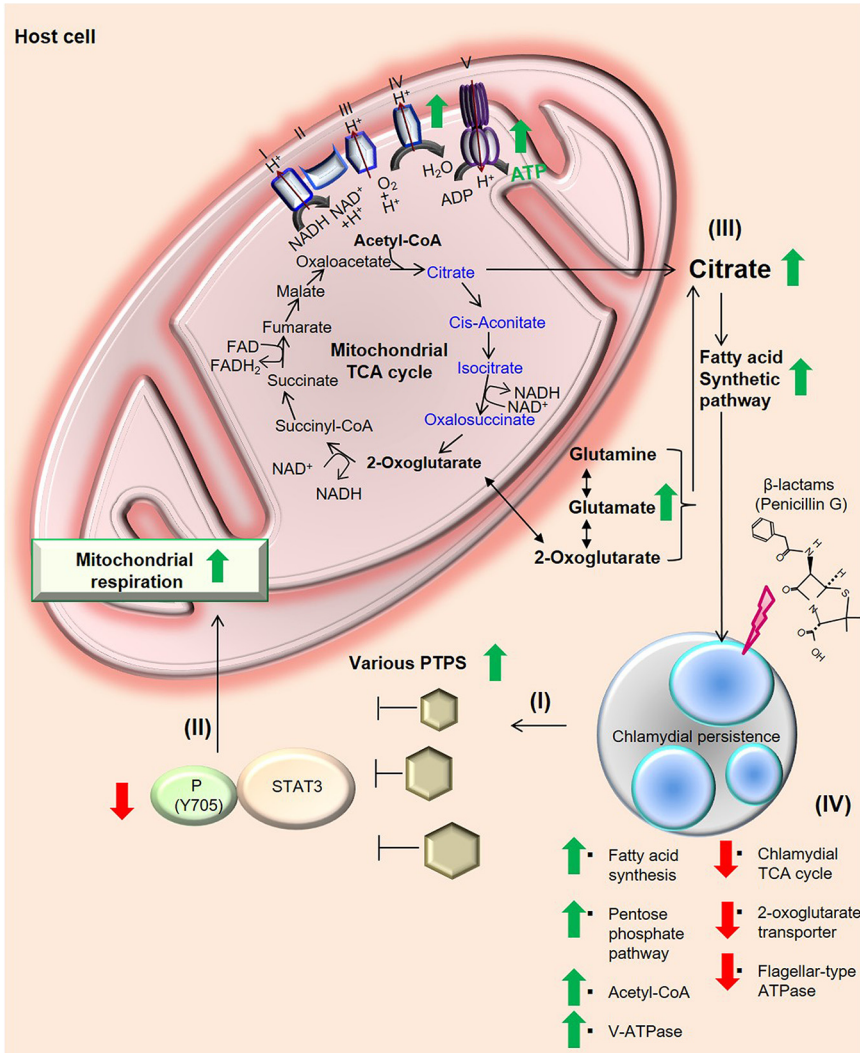


**FIG 5** Impact of mitochondrial activity on chlamydial metabolism in  $\beta$ -lactam-induced persistent infection. (I)  $\beta$ -Lactam-induced persistent *C. trachomatis* inactivates STAT3 by increased host PTPs in epithelial cells. (II) Reduced STAT3 activity functions to accelerate mitochondrial respiration. (III) Activated mitochondria and glutamine metabolism can enhance the production of citrate that can be utilized for host and chlamydial fatty acid/phospholipid synthesis in penicillin-induced chlamydial persistence. (IV) Chlamydial metabolism switched from the tricarboxylic acid cycle to fatty acid synthesis in  $\beta$ -lactam-induced persistent infection. Green arrows indicate upregulation, and red arrows indicate downregulation. Metabolites denoted in blue in the mitochondrial TCA cycle cannot be synthesized in the chlamydial TCA cycle because *C. trachomatis* lacks metabolic genes encoding citrate synthase, aconitate hydratase, and isocitrate dehydrogenase.

undergo metabolic reprogramming to persist in the presence of  $\beta$ -lactam antimicrobials (Fig. 5).

**MATERIALS AND METHODS**

**Chemicals and antibodies.** Chemicals were purchased from either Sigma-Aldrich (Deisenhofen, Germany), New England BioLabs GmbH (Frankfurt am Main, Germany), or MedKoo Biosciences, Inc. (Morrisville, NC). Rabbit anti-glyceraldehyde-3-phosphate dehydrogenase (GAPDH), rabbit anti-phospho-Stat3 (Y705), rabbit anti-phospho-Stat3 (S727), rabbit anti-SOCS3, rabbit anti-ACL, rabbit anti-phospho-ACL (S455), rabbit anti-ACSL1, rabbit anti-AceCS1, horseradish peroxidase (HRP)-horse anti-mouse IgG, and HRP-goat anti-rabbit IgG were purchased from Cell Signaling Technology (Frankfurt am Main, Germany). A total oxidative phosphorylation (OXPHOS) rodent Western blot (WB) antibody cocktail was purchased from Abcam (Cambridge, UK). Rabbit anti-STAT3 was purchased from Proteintech Group (Chicago, IL). Two different Stealth RNAi siRNAs for STAT3 (STAT3HSS186130 and STAT3HSS186131) were purchased from Invitrogen (Karlsruhe, Germany).



**Bacterial strains and host cells.** Since the prevalence of urogenital *C. trachomatis* is caused by serovars D to F, we performed our experiments using *C. trachomatis* serovar D (ATCC VR885) in this study. HeLa cells (ATCC CCL-2) and primary fibroblasts isolated from C57BL/6J mice (kindly provided from Saleh M. Ibrahim, Lübeck Institute of Experimental Dermatology, University of Lübeck) were used as host cells.

**Cell culture.** All experiments except for the experiment using primary fibroblasts were performed with RPMI 1640 medium supplemented with 5% fetal bovine serum (FBS) (Invitrogen), nonessential amino acids (Gibco/Thermo Fisher Scientific, Waltham, MA), and 2 mM glutamine (Lonza, Walkersville, MD). Dulbecco's modified Eagle's medium (DMEM) containing 10% FBS and 2 mM glutamine was used for the culture of primary fibroblast cells. Penicillin G (1 U/ml) or a therapeutically relevant serum concentration of amoxicillin (11  $\mu$ g/ml) (7) (Sigma-Aldrich) was added at the time of infection to induce chlamydial persistence. For IFN- $\gamma$ -induced persistence, 50 U/ml IFN- $\gamma$  was added to the cells 24 h prior to infection.

**XF Cell Mito stress test.** A total of  $1.5 \times 10^4$  HeLa cells were infected with *C. trachomatis* (0.7 inclusion-forming units [IFU]/cell) in 24-well XF plates (Seahorse Bioscience, Copenhagen, Denmark). The cells were centrifuged at  $700 \times g$  for 1 h at 35°C and incubated for 24 h. Afterwards, the Mito stress test kit (Seahorse Bioscience) was used according to the manufacturer's instructions with the chemicals oligomycin (0.5  $\mu$ M), carbonyl cyanide-4-(trifluoromethoxy)phenylhydrazone (FCCP) (0.2  $\mu$ M), and antimycin A (1  $\mu$ M) plus rotenone (1  $\mu$ M). In the preliminary experiment, we confirmed that the oligomycin concentration that was used for the XF Cell Mito stress assay had no effect on chlamydial progeny. After the assay, cells from productive infection and chlamydial persistence were fixed with methanol for 10 min at -20°C. Cells were then incubated for 20 min with fluorescein isothiocyanate (FITC)-labeled monoclonal chlamydial lipooligosaccharide (LOS) antibodies (Dako, Glostrup, Denmark). Evans blue counterstaining of host cells was used for better characterization of intracellular inclusions. Staining was confirmed by using a Keyence (Osaka, Japan) BZ-9000 instrument.

**Western blot analysis.** To determine the amount of STAT3 pY<sup>705</sup>,  $0.2 \times 10^5$  to  $5.3 \times 10^5$  HeLa or primary fibroblast cells were seeded in 6- or 96-well plates (Greiner Bio-One, Frickenhausen, Germany) and infected with *C. trachomatis* (0.7 IFU/cell). *C. trachomatis*-infected cells were lysed with 8 M urea supplemented with 325 U/ml Benzonase nuclease (Sigma-Aldrich) at the indicated times. Cell lysates were diluted into Laemmli buffer (50 mM Tris-HCl [pH 6.8], 2% SDS, 1% 2-mercaptoethanol, 10% glycerol, 0.1% bromophenol blue). On the other hand, we used lysis buffer with bromophenol blue (125 mM Tris-HCl [pH 7.8], 4% SDS, 0.1 M dithiothreitol [DTT], 20% glycerol) to check STAT3 knockdown efficacy. Samples were analyzed by Western blot analysis (Bio-Rad, Hercules, CA) and visualized using enhanced chemiluminescence (ECL) reagent (Millipore and Thermo Fisher Scientific). Images were acquired by using the Fusion FX7 system (Vilber Lourmat, Eberhardzell, Germany), and the density of each band was measured by using Bio-1D software (Vilber Lourmat).

**Electron microscopy.** A total of  $5.3 \times 10^5$  cells were infected with *C. trachomatis* (0.7 IFU/cell). *C. trachomatis*-infected cells were fixed with 2% paraformaldehyde and 2.5% glutaraldehyde in 0.1 M cacodylate buffer for 1 h. Postfixation was performed with 1% OsO<sub>4</sub> in 0.1 M cacodylate buffer for 2 h. Samples were dehydrated with a graded ethanol series and embedded in Araldite (Fluka, Buchs, Switzerland). Ultrathin sections were stained with uranyl acetate and lead citrate and examined with a JEOL 1011 transmission electron microscope (JEOL, Tokyo, Japan).

**Recovery and reactivation assays of  $\beta$ -lactam-induced persistent *C. trachomatis* infection.** A total of  $1 \times 10^5$  HeLa cells were infected with 0.7 IFU/cell of *C. trachomatis*. *C. trachomatis*-infected cells were treated with or without 1 U/ml penicillin or 11  $\mu$ g/ml amoxicillin at the time of infection to induce chlamydial persistence (see Fig. S2D in the supplemental material). The plate was further centrifuged at  $700 \times g$  for 1 h at 35°C and incubated for 24 h. For reactivation of persistent *C. trachomatis*, medium was changed to fresh medium in the absence of antimicrobials, and cells were incubated for another 48 h. Afterwards, *C. trachomatis*-infected cells were harvested, disrupted with glass beads, and inoculated onto  $3 \times 10^5$  HEp-2 cells (ATCC CCL-23). *C. trachomatis* infection was visualized by immunofluorescence staining with a mouse anti-chlamydial LOS antibody (kindly provided by Helmut Brade, Borstel, Germany). Chlamydial inclusions were visualized with a Keyence (Osaka, Japan) BZ9000 instrument.

**RNA interference.** Transfection was performed according to the manufacturer's guidelines (Invitrogen), and STAT3 was transiently silenced by transfection of specific siRNA.

In brief,  $2.5 \times 10^4$  HeLa cells were seeded into 96-well plates. A mixture of 5  $\mu$ l Opti-MEM (Invitrogen), 0.2  $\mu$ l Lipofectamine 2000 (Invitrogen), and 30 nM siRNA was added to cells. The same amount of the negative-control low-GC-content duplex (Invitrogen) was used for the control. After 4 h of incubation, 150  $\mu$ l RPMI 1640 medium including 5% FBS was added.

**Infection rate and recovery assays in STAT3 knockdown cells.** A total of  $5.3 \times 10^5$  HeLa cells were infected with *C. trachomatis* (0.7 IFU/cell) at posttransfection. The plate was further centrifuged at  $700 \times g$  for 1 h at 35°C and incubated at 37°C under a 5% CO<sub>2</sub> atmosphere. Afterwards, *C. trachomatis* infection was analyzed by immunofluorescence staining with mouse anti-chlamydial LOS antibody (green), which was used to visualize chlamydial inclusions (BZ9000; Keyence, Osaka, Japan). Evans blue counterstaining of host cells (red) was used for counting cell numbers. The numbers of recoverable *C. trachomatis* cells in STAT3 knockdown cells were normalized to those of siRNA control cells.

**Two-photon microscopy.** NAD(P)H autofluorescence was imaged with the Dermalnspect two-photon laser scanning microscope (Jen-Lab GmbH, Jena, Germany) (40). In brief, cells were infected with *C. trachomatis* (0.7 IFU/cell) on cover glass in 50-mm culture dishes with or without penicillin. The cover glass was transferred into a MiniCem chamber before the assay. In each cell, the fluorescence lifetime of protein-bound NAD(P)H [ $\tau_2$ -NAD(P)H] was measured at 24 and 36 hpi. A 40 $\times$ /1.3 Plan-Apochromat oil

immersion objective was used for visualization. An excitation source at 730 nm was used to measure the fluorescence lifetime of NAD(P)H. The fluorescence lifetime was detected over a period of 49.7 s per image using a time-correlated single-photon counting (TCSPC) system. Afterwards, the data were analyzed by using SPCImage software version 2.9.5.2996 (Becker & Hickl GmbH, Berlin, Germany). In every picture, three inclusions were analyzed from 10 visual fields per chamber in three independent measurements. A region of interest (ROI) was selected inside the whole chlamydial inclusions. Mean values of  $\tau_2$ -NAD(P)H of all pixels inside the ROI were calculated.

**NMR analysis.** HeLa cells were infected with *C. trachomatis* (0.7 IFU/cell) in 6-well plates and cultured in RPMI 1640 medium supplemented with 5% fetal bovine serum with or without 1 U/ml penicillin. The plate was incubated for 24 h at 37°C under a 5% CO<sub>2</sub> atmosphere. Afterwards, the cells were washed with phosphate-buffered saline (PBS) twice and harvested. For each sample,  $5 \times 10^6$  cells were used for NMR analysis. Cell extracts were dissolved in pH 7 phosphate buffer with 0.5 mM deuterated TMSP [3-(trimethylsilyl)-2,2,3,3-tetradeuteropropionic acid] as a chemical shift and concentration reference, as described previously (68). Samples were analyzed using a Bruker Avance III 600-MHz nuclear magnetic resonance spectrometer with a room-temperature HCN probe (Bruker). One-dimensional (1D) spectra were acquired using a 1D nuclear Overhauser effect spectroscopy (1D-NOESY) pulse sequence with water presaturation (noesygppr1d), using 1,024 scans, a recycle delay of 4 s, a sweep width of 12 ppm, and 32,768 data points for acquisition. Metabolite concentrations were measured using Chenomx software (version 8.5) and MetaboLab/NMRLab (69, 70). In addition, reference spectra of 2-oxoglutarate, glutamine, glutamate, as well as citrate were acquired in the same buffer.

**Transcriptome analysis.** A total of  $2.5 \times 10^5$  cells were seeded into 6-well plates and infected with *C. trachomatis*. Total RNA isolation was performed with the NucleoSpin RNA kit (Macherey-Nagel GmbH & Co. KG, Düren, Germany). Human rRNA was depleted from each sample using Ribo-Zero rRNA removal (human/mouse/rat) kits (Epicentre, Chicago, IL). Afterwards, the obtained human rRNA-depleted RNA was purified with the NucleoSpin RNA kit (Macherey-Nagel) according to the RNA purification protocol. rRNA depletion was checked by Bioanalyzer RNA6000 Pico chip analyses (Agilent Technologies). Depleted RNA preparations were quantified by fluorometric Qubit RNA assays (Life Technologies).

Syntheses of cDNA libraries were performed according to the manufacturer's protocol (TruSeq RNA sample prep kit; Illumina, Inc.), with minor modifications. Briefly, 45 to 100 ng of human rRNA-depleted RNA was used for cDNA synthesis, followed by adapter ligation and PCR amplification. The resulting cDNA libraries were validated by Agilent DNA 1000 chip analysis (Agilent Technologies), quantified by fluorometric measurement (Qubit high-sensitivity double-stranded DNA [dsDNA HS] assay kit; Life Technologies), and adjusted to 10 nM.

Clonal amplification of cDNA on Illumina v3 flow cells was done using the appropriate cBot recipe (version 8) at a final library concentration of 10 pM. Sequencing was carried out on a HiSeq2500 system according to the manufacturer's protocol (HiSeq2500 system user guide; Illumina, Inc.) using TruSeq SBS v3 chemistry (Illumina, Inc.). The resulting 100-bp sequence reads were converted to fastq format by using CASAVA 1.8.2.

The sequenced cDNA reads of each sample were analyzed via Babraham Bioinformatics FastQC, a quality control tool for high-throughput sequence data (version 0.11.4; <https://www.bioinformatics.babraham.ac.uk/projects/fastqc/>). Quality trimming and filtering as well as length filtering were done with PRINSEQ-lite (version 0.20.4). The remaining high-quality sequence reads were mapped against the human reference genome (Genome Reference Consortium human build 38 patch release 2 [GRCh38.p2] [accession number GCF\_000001405.28]) and the *C. trachomatis* D/UW-3/CX reference genome (accession number GCF\_000008725.1) combined with the sequence of *C. trachomatis* D/SotonD1 plasmid pSotonD1 (NCBI reference sequence accession number NC\_020986.1) using BWA (version 0.7.17) (71). The mapped reads per *Chlamydia* gene were extracted with featureCounts (version 1.6.0) (72). Normalization and differential expression analysis were done with DESeq2 (71), and as a threshold for differentially expressed genes, an adjusted *P* value of  $\leq 0.05$  was used.

**qPCR for analysis of chlamydial gene expression.** A total of  $2.5 \times 10^5$  cells were seeded in 6-well plates and cultured for 24 h or 18 h. Extraction of total RNA and reverse transcription to cDNA were performed. A LightCycler detection system (Roche Molecular Biochemicals, Mannheim, Germany) was used to perform qPCR. The relative quantification of chlamydial target mRNA expression levels was normalized by chlamydial 16S using the threshold cycle ( $2^{\Delta\Delta CT}$ ) method. The primer sequences are listed in Table S3. Statistics were performed with paired Student's *t* test.

**Expression of PTPs.** A total of  $0.3 \times 10^5$  to  $5.3 \times 10^5$  HeLa or primary fibroblast cells were seeded in 6- or 96-well plates. Cells were infected with *C. trachomatis* (0.7 IFU/cell). PTP expression levels were determined by qPCR as described above. PTP expression levels were normalized by the endogenous control  $\beta$ -actin gene. Primers for PTPN2, PTPN9, PTPN11, PTPN6, PTPRK, PTPRD, and PTPRT were purchased from Bio-Rad Laboratories GmbH (Feldkirchen, Germany).

**Effect of the PTP inhibitor on the phosphorylation of STAT3.** A total of  $5.3 \times 10^5$  cells were seeded in 6-well plates and cultured for 24 h. Cells were infected with *C. trachomatis* (0.7 IFU/cell) and centrifuged at  $700 \times g$  for 1 h at 35°C. Infected cells were incubated at 37°C under a 5% CO<sub>2</sub> atmosphere for 24 h. Afterwards, they were treated with or without 25  $\mu$ M sodium orthovanadate (New England Biolabs GmbH) for 3 h.

**Effect of chlamydial FabI and host fatty acid synthetic inhibitors.** A total of  $1 \times 10^5$  cells were infected with *C. trachomatis* (0.7 IFU/cell) in the presence or absence of AFN-1252 (MedKoo Biosciences, Inc.). The plate was centrifuged at  $700 \times g$  for 1 h at 35°C and incubated at 37°C under a 5% CO<sub>2</sub> atmosphere. The host fatty acid synthetic inhibitor C75 (20  $\mu$ g/ml) (Sigma-Aldrich) was added at 12 hpi and further incubated for 12 h. Afterwards, *C. trachomatis*-infected cells were used for immunofluorescence

staining with FITC-labeled monoclonal chlamydial LOS antibodies (Dako). A Keyence BZ9000 instrument was used to measure the diameter of chlamydial inclusions.

**Determination of protein concentrations.** A micro-bicinchoninic acid (BCA) protein assay kit (Thermo Fisher Scientific) was used according to the manufacturer's instructions. In brief, cells were harvested and washed twice in PBS. After centrifugation for 5 min at  $300 \times g$ , the cell pellet was resuspended in lysis buffer (20 mM HEPES, 150 mM NaCl, 1% Triton X-100, 10% glycerol, protein inhibitor cocktail) and sonicated 3 times for 5 s. After sonication, another centrifugation step followed at  $15,000 \times g$  for 15 min at 4°C. When the supernatant was collected and used for spectrophotometric analysis to determine the total protein concentration, we confirmed no significant difference in the protein concentrations in C75-treated cells ( $n=4$ ; mean  $\pm$  standard error of the mean [SEM]; Sidak's multiple-comparison test).

**Statistics.** Data are indicated as means  $\pm$  SEM. Statistical analysis was performed by using GraphPad Prism 7 statistical software. When three or more groups were compared in the experiment, Sidak's multiple-comparison test was used in cases where one-way analysis of variance showed statistically significant differences ( $P$  values of  $\leq 0.05$ ). Data between two groups were evaluated using Student's  $t$  test. In Sidak's multiple-comparison and Student's  $t$  tests,  $P$  values of  $\leq 0.05$  were considered statistically significant.

**Data availability.** All raw RNA-seq data sets were deposited in the National Center for Biotechnology (NCBI) Sequence Read Archive (SRA) under BioProject accession number [PRJNA378340](https://www.ncbi.nlm.nih.gov/bioproject/PRJNA378340) with SRA accession numbers [SRR5834399](https://www.ncbi.nlm.nih.gov/sra/SRR5834399) and [SRR5834397](https://www.ncbi.nlm.nih.gov/sra/SRR5834397) (productive infection), [SRR5834400](https://www.ncbi.nlm.nih.gov/sra/SRR5834400) and [SRR5834398](https://www.ncbi.nlm.nih.gov/sra/SRR5834398) (penicillin-induced persistence), and [SRR13189638](https://www.ncbi.nlm.nih.gov/sra/SRR13189638) and [SRR13189738](https://www.ncbi.nlm.nih.gov/sra/SRR13189738) (IFN- $\gamma$ -induced persistence).

## SUPPLEMENTAL MATERIAL

Supplemental material is available online only.

**FIG S1**, TIF file, 1.2 MB.

**FIG S2**, TIF file, 2 MB.

**FIG S3**, TIF file, 1.4 MB.

**FIG S4**, TIF file, 2.6 MB.

**FIG S5**, TIF file, 2.2 MB.

**TABLE S1**, XLSX file, 0.1 MB.

**TABLE S2**, XLSX file, 0.04 MB.

**TABLE S3**, XLSX file, 0.01 MB.

## ACKNOWLEDGMENTS

We gratefully thank Siegrid Pätzmann, Kristin Wischnat, Anke Hellberg, and Marie Kleingarn (Department of Infectious Diseases and Microbiology, University of Lübeck); Jutta Endler and Christo Orün (Institute of Anatomy, University of Lübeck); Christina Zechel (Department of Neurosurgery, University of Lübeck); and Evelyn Wachholz (Institute of Chemistry and Metabolomics, University of Lübeck) for technical assistance. We also thank Gereon Hüttmann and Yoko Miura (Institute of Biomedical Optics, University of Lübeck) for their valuable advice about two-photon microscopy and image analysis and Saleh M. Ibrahim and Misa Hirose (Lübeck Institute of Experimental Dermatology, University of Lübeck) for providing primary mouse fibroblasts. Two-photon imaging was enabled by the Small Animal Imaging Facility Lübeck (SAIL).

This work was supported by ERA-NET PathoGenoMics (Pathomics) (0315442C), the German Research Foundation (DFG) (KA4420/1-1), DFG-funded International Research Training Group (IRTG) 1911 (project B 8.1), the University of Lübeck (P01-2012 and E10-2013), and the German Center for Infection Research (DZIF) (TI07.003/80115MDMAW/FKZ 80002043).

## REFERENCES

- Woodhall SC, Gorwitz RJ, Migchelsen SJ, Gottlieb SL, Horner PJ, Geisler WM, Winstanley C, Hufnagel K, Waterboer T, Martin DL, Huston WM, Gaydos CA, Deal C, Unemo M, Dunbar JK, Bernstein K. 2018. Advancing the public health applications of *Chlamydia trachomatis* serology. *Lancet Infect Dis* 18:e399–e407. [https://doi.org/10.1016/S1473-3099\(18\)30159-2](https://doi.org/10.1016/S1473-3099(18)30159-2).
- Omsland A, Sager J, Nair V, Sturdevant DE, Hackstadt T. 2012. Developmental stage-specific metabolic and transcriptional activity of *Chlamydia trachomatis* in an axenic medium. *Proc Natl Acad Sci U S A* 109:19781–19785. <https://doi.org/10.1073/pnas.1212831109>.
- Wyrick PB, Knight ST. 2004. Pre-exposure of infected human endometrial epithelial cells to penicillin in vitro renders *Chlamydia trachomatis* refractory to azithromycin. *J Antimicrob Chemother* 54:79–85. <https://doi.org/10.1093/jac/dkh283>.
- Storey C, Chopra I. 2001. Affinities of beta-lactams for penicillin binding proteins of *Chlamydia trachomatis* and their antichlamydial activities. *Antimicrob Agents Chemother* 45:303–305. <https://doi.org/10.1128/AAC.45.1.303-305.2001>.
- Lewis ME, Belland RJ, AbdelRahman YM, Beatty WL, Aiyar AA, Zea AH, Greene SJ, Marrero L, Buckner LR, Tate DJ, McGowin CL, Kozlowski PA,

- O'Brien M, Lillis RA, Martin DH, Quayle AJ. 2014. Morphologic and molecular evaluation of Chlamydia trachomatis growth in human endocervix reveals distinct growth patterns. *Front Cell Infect Microbiol* 4:71. <https://doi.org/10.3389/fcimb.2014.00071>.
6. Phillips Campbell R, Kintner J, Whittimore J, Schoborg RV. 2012. Chlamydia muridarum enters a viable but non-infectious state in amoxicillin-treated BALB/c mice. *Microbes Infect* 14:1177–1185. <https://doi.org/10.1016/j.micinf.2012.07.017>.
  7. Kintner J, Lajoie D, Hall J, Whittimore J, Schoborg RV. 2014. Commonly prescribed  $\beta$ -lactam antibiotics induce C. trachomatis persistence/stress in culture at physiologically relevant concentrations. *Front Cell Infect Microbiol* 4:44. <https://doi.org/10.3389/fcimb.2014.00044>.
  8. Su H, Caldwell HD. 1995. CD4+ T cells play a significant role in adoptive immunity to Chlamydia trachomatis infection of the mouse genital tract. *Infect Immun* 63:3302–3308. <https://doi.org/10.1128/IAI.63.9.3302-3308.1995>.
  9. Belland RJ, Nelson DE, Virok D, Crane DD, Hogan D, Sturdevant D, Beatty WL, Caldwell HD. 2003. Transcriptome analysis of chlamydial growth during IFN-gamma-mediated persistence and reactivation. *Proc Natl Acad Sci U S A* 100:15971–15976. <https://doi.org/10.1073/pnas.2535394100>.
  10. Shima K, Kaeding N, Ogunsulire IM, Kaufhold I, Klinger M, Rupp J. 2018. Interferon- $\gamma$  interferes with host cell metabolism during intracellular Chlamydia trachomatis infection. *Cytokine* 112:95–101. <https://doi.org/10.1016/j.cyto.2018.05.039>.
  11. Matsumoto A, Manire GP. 1970. Electron microscopic observations on the effects of penicillin on the morphology of Chlamydia psittaci. *J Bacteriol* 101:278–285. <https://doi.org/10.1128/JB.101.1.278-285.1970>.
  12. Clark RB, Schatzki PF, Dalton HP. 1982. Ultrastructural effect of penicillin and cycloheximide on Chlamydia trachomatis strain HAR-13. *Med Microbiol Immunol* 171:151–159. <https://doi.org/10.1007/BF02123623>.
  13. Skilton RJ, Cutcliffen LT, Barlow D, Wang Y, Salim O, Lambden PR, Clarke IN. 2009. Penicillin induced persistence in Chlamydia trachomatis: high quality time lapse video analysis of the developmental cycle. *PLoS One* 4:e7723. <https://doi.org/10.1371/journal.pone.0007723>.
  14. Workowski KA, Bolan GA, Centers for Disease Control and Prevention. 2015. Sexually transmitted diseases treatment guidelines, 2015. *MMWR Recommend Rep* 64:1–137.
  15. World Health Organization. 2016. WHO guidelines for the treatment of Chlamydia trachomatis. World Health Organization, Geneva, Switzerland.
  16. Hicks LA, Bartoces MG, Roberts RM, Suda KJ, Hunkler RJ, Taylor TH, Jr, Schrag SJ. 2015. US outpatient antibiotic prescribing variation according to geography, patient population, and provider specialty in 2011. *Clin Infect Dis* 60:1308–1316. <https://doi.org/10.1093/cid/civ076>.
  17. Reveneau N, Crane DD, Fischer E, Caldwell HD. 2005. Bactericidal activity of first-choice antibiotics against gamma interferon-induced persistent infection of human epithelial cells by Chlamydia trachomatis. *Antimicrob Agents Chemother* 49:1787–1793. <https://doi.org/10.1128/AAC.49.5.1787-1793.2005>.
  18. Liechti GW, Kuru E, Hall E, Kalinda A, Brun YV, VanNieuwenhze M, Maurelli AT. 2014. A new metabolic cell-wall labelling method reveals peptidoglycan in Chlamydia trachomatis. *Nature* 506:507–510. <https://doi.org/10.1038/nature12892>.
  19. Klöckner A, Otten C, Derouaux A, Vollmer W, Bühl H, De Benedetti S, Münch D, Josten M, Mölleken K, Sahl H-G, Henrichfreise B. 2014. AmiA is a penicillin target enzyme with dual activity in the intracellular pathogen Chlamydia pneumoniae. *Nat Commun* 5:4201. <https://doi.org/10.1038/ncomms5201>.
  20. Cox JV, Abdelrahman YM, Ouellette SP. 2020. Penicillin-binding proteins regulate multiple steps in the polarized cell division process of Chlamydia. *Sci Rep* 10:12588. <https://doi.org/10.1038/s41598-020-69397-x>.
  21. Chowdhury SR, Reimer A, Sharan M, Kozjak-Pavlovic V, Eulalio A, Prusty BK, Fraunholz M, Karunakaran K, Rudel T. 2017. Chlamydia preserves the mitochondrial network necessary for replication via microRNA-dependent inhibition of fission. *J Cell Biol* 216:1071–1089. <https://doi.org/10.1083/jcb.201608063>.
  22. Stephens RS, Kalman S, Lammel C, Fan J, Marathe R, Aravind L, Mitchell W, Olinger L, Tatusov RL, Zhao Q, Koonin EV, Davis RW. 1998. Genome sequence of an obligate intracellular pathogen of humans: Chlamydia trachomatis. *Science* 282:754–759. <https://doi.org/10.1126/science.282.5389.754>.
  23. Kubo A, Stephens RS. 2001. Substrate-specific diffusion of select dicarboxylates through Chlamydia trachomatis PorB. *Microbiology (Reading)* 147:3135–3140. <https://doi.org/10.1099/00221287-147-11-3135>.
  24. Rajeeve K, Vollmuth N, Janaki-Raman S, Wulff TF, Baluapuri A, Dejure FR, Huber C, Fink J, Schmalhofer M, Schmitz W, Sivadasan R, Eilers M, Wolf E, Eisenreich W, Schulze A, Seibel J, Rudel T. 2020. Reprogramming of host glutamine metabolism during Chlamydia trachomatis infection and its key role in peptidoglycan synthesis. *Nat Microbiol* 5:1390–1402. <https://doi.org/10.1038/s41564-020-0762-5>.
  25. Zaidi N, Swinnen JV, Smans K. 2012. ATP-citrate lyase: a key player in cancer metabolism. *Cancer Res* 72:3709–3714. <https://doi.org/10.1158/0008-5472.CAN-11-4112>.
  26. Yao J, Cherian PT, Frank MW, Rock CO. 2015. Chlamydia trachomatis relies on autonomous phospholipid synthesis for membrane biogenesis. *J Biol Chem* 290:18874–18888. <https://doi.org/10.1074/jbc.M115.657148>.
  27. Yao J, Dodson VJ, Frank MW, Rock CO. 2015. Chlamydia trachomatis scavenges host fatty acids for phospholipid synthesis via an acyl-acyl carrier protein synthetase. *J Biol Chem* 290:22163–22173. <https://doi.org/10.1074/jbc.M115.671008>.
  28. Yao J, Abdelrahman YM, Robertson RM, Cox JV, Belland RJ, White SW, Rock CO. 2014. Type II fatty acid synthesis is essential for the replication of Chlamydia trachomatis. *J Biol Chem* 289:22365–22376. <https://doi.org/10.1074/jbc.M114.584185>.
  29. Van Ooij C, Kalman L, Van Ijzendoorn S, Nishijima M, Hanada K, Mostov K, Engel JN. 2000. Host cell-derived sphingolipids are required for the intracellular growth of Chlamydia trachomatis. *Cell Microbiol* 2:627–637. <https://doi.org/10.1046/j.1462-5822.2000.00077.x>.
  30. Elwell CA, Jiang S, Kim JH, Lee A, Wittmann T, Hanada K, Melancon P, Engel JN. 2011. Chlamydia trachomatis co-opts GBF1 and CERT to acquire host sphingomyelin for distinct roles during intracellular development. *PLoS Pathog* 7:e1002198. <https://doi.org/10.1371/journal.ppat.1002198>.
  31. Derré I, Swiss R, Agaisse H. 2011. The lipid transfer protein CERT interacts with the Chlamydia inclusion protein IncD and participates to ER-Chlamydia inclusion membrane contact sites. *PLoS Pathog* 7:e1002092. <https://doi.org/10.1371/journal.ppat.1002092>.
  32. Vromman F, Subtil A. 2014. Exploitation of host lipids by bacteria. *Curr Opin Microbiol* 17:38–45. <https://doi.org/10.1016/j.mib.2013.11.003>.
  33. Sala D, Cunningham TJ, Stec MJ, Etxaniz U, Nicoletti C, Dall'Agnese A, Puri PL, Duester G, Latella L, Sacco A. 2019. The Stat3-Fam3a axis promotes muscle stem cell myogenic lineage progression by inducing mitochondrial respiration. *Nat Commun* 10:1796. <https://doi.org/10.1038/s41467-019-09746-1>.
  34. Demaria M, Giorgi C, Lebedzinska M, Esposito G, D'Angeli L, Bartoli A, Gough DJ, Turkson J, Levy DE, Watson CJ, Wieckowski MR, Provero P, Pinton P, Poli V. 2010. A STAT3-mediated metabolic switch is involved in tumour transformation and STAT3 addiction. *Aging (Albany NY)* 2:823–842. <https://doi.org/10.18632/aging.100232>.
  35. Camporeale A, Demaria M, Monteleone E, Giorgi C, Wieckowski MR, Pinton P, Poli V. 2014. STAT3 activities and energy metabolism: dangerous liaisons. *Cancers (Basel)* 6:1579–1596. <https://doi.org/10.3390/cancers6031579>.
  36. Pensa S, Demaria M, Avalle L, Barbieri I, Camporeale A, Poli V. 2012. From tissue invasion to glucose metabolism: the many aspects of signal transducer and activator of transcription 3 pro-oncogenic activities. *Horm Mol Biol Clin Invest* 10:217–225. <https://doi.org/10.1515/hmbci-2012-0006>.
  37. Wegryzn J, Potla R, Chwae Y-J, Sepuri NBV, Zhang Q, Koeck T, Derecka M, Szczepanek K, Szelag M, Gornicka A, Moh A, Moghaddas S, Chen Q, Bobbili S, Cichy J, Dulak J, Baker GP, Wolfman A, Stuehr D, Hassan MO, Fu X-Y, Avadhani N, Drake JI, Fawcett P, Lesnefsky EJ, Larner AC. 2009. Function of mitochondrial Stat3 in cellular respiration. *Science* 323:793–797. <https://doi.org/10.1126/science.1164551>.
  38. Kim M, Morales LD, Jang I-S, Cho Y-Y, Kim DJ. 2018. Protein tyrosine phosphatases as potential regulators of STAT3 signaling. *Int J Mol Sci* 19:2708. <https://doi.org/10.3390/ijms19092708>.
  39. Shuai K, Liu B. 2003. Regulation of JAK-STAT signalling in the immune system. *Nat Rev Immunol* 3:900–911. <https://doi.org/10.1038/nri1226>.
  40. Szaszák M, Steven P, Shima K, Orzekowsky-Schröder R, Hüttmann G, König IR, Solbach W, Rupp J. 2011. Fluorescence lifetime imaging unravels C. trachomatis metabolism and its crosstalk with the host cell. *PLoS Pathog* 7:e1002108. <https://doi.org/10.1371/journal.ppat.1002108>.
  41. Beatty WL, Morrison RP, Byrne GI. 1994. Persistent chlamydiae: from cell culture to a paradigm for chlamydial pathogenesis. *Microbiol Rev* 58:686–699. <https://doi.org/10.1128/MR.58.4.686-699.1994>.
  42. Schoborg RV. 2011. Chlamydia persistence—a tool to dissect chlamydia-host interactions. *Microbes Infect* 13:649–662. <https://doi.org/10.1016/j.micinf.2011.03.004>.
  43. Beatty WL, Byrne GI, Morrison RP. 1993. Morphologic and antigenic characterization of interferon gamma-mediated persistent Chlamydia



- trachomatis infection in vitro. *Proc Natl Acad Sci U S A* 90:3998–4002. <https://doi.org/10.1073/pnas.90.9.3998>.
44. Loomis WP, Starnbach MN. 2002. T cell responses to *Chlamydia trachomatis*. *Curr Opin Microbiol* 5:87–91. [https://doi.org/10.1016/s1369-5274\(02\)00291-6](https://doi.org/10.1016/s1369-5274(02)00291-6).
  45. Mashima T, Seimiya H, Tsuruo T. 2009. De novo fatty-acid synthesis and related pathways as molecular targets for cancer therapy. *Br J Cancer* 100:1369–1372. <https://doi.org/10.1038/sj.bjc.6605007>.
  46. Sadowski MC, Pouwer RH, Gunter JH, Lubik AA, Quinn RJ, Nelson CC. 2014. The fatty acid synthase inhibitor triclosan: repurposing an anti-microbial agent for targeting prostate cancer. *Oncotarget* 5:9362–9381. <https://doi.org/10.18632/oncotarget.2433>.
  47. Kiriya Y, Nochi H. 2018. Intra- and intercellular quality control mechanisms of mitochondria. *Cells* 7:1. <https://doi.org/10.3390/cells7010001>.
  48. Lin T, Bost KL. 2004. STAT3 activation in macrophages following infection with *Salmonella*. *Biochem Biophys Res Commun* 321:828–834. <https://doi.org/10.1016/j.bbrc.2004.07.039>.
  49. Zhao J, Dong Y, Kang W, Go MY, Tong JH, Ng EK, Chiu PW, Cheng AS, To KF, Sung JJ, Yu J. 2014. *Helicobacter pylori*-induced STAT3 activation and signalling network in gastric cancer. *Oncoscience* 1:468–475. <https://doi.org/10.18632/oncoscience.62>.
  50. Queval CJ, Song O-R, Deboosère N, Delorme V, Debrie A-S, Iantomasi R, Veyron-Churllet R, Jouny S, Redhage K, Deloison G, Baulard A, Chamaillard M, Loch C, Brodin P. 2016. STAT3 represses nitric oxide synthesis in human macrophages upon *Mycobacterium tuberculosis* infection. *Sci Rep* 6:29297. <https://doi.org/10.1038/srep29297>.
  51. Chang Z, Wang Y, Zhou X, Long J-E. 2018. STAT3 roles in viral infection: antiviral or proviral? *Future Virol* 13:557–574. <https://doi.org/10.2217/fvl-2018-0033>.
  52. Mizutani T, Fukushi S, Murakami M, Hirano T, Saijo M, Kurane I, Morikawa S. 2004. Tyrosine dephosphorylation of STAT3 in SARS coronavirus-infected Vero E6 cells. *FEBS Lett* 577:187–192. <https://doi.org/10.1016/j.febslet.2004.10.005>.
  53. Sun S, Steinberg BM. 2002. PTEN is a negative regulator of STAT3 activation in human papillomavirus-infected cells. *J Gen Virol* 83:1651–1658. <https://doi.org/10.1099/0022-1317-83-7-1651>.
  54. Xu Y, Fisher GJ. 2012. Receptor type protein tyrosine phosphatases (RTPs)—roles in signal transduction and human disease. *J Cell Commun Signal* 6:125–138. <https://doi.org/10.1007/s12079-012-0171-5>.
  55. Stumvoll M, Perriello G, Meyer C, Gerich J. 1999. Role of glutamine in human carbohydrate metabolism in kidney and other tissues. *Kidney Int* 55:778–792. <https://doi.org/10.1046/j.1523-1755.1999.055003778.x>.
  56. Yang M, Rajeeve K, Rudel T, Dandekar T. 2019. Comprehensive flux modeling of *Chlamydia trachomatis* proteome and qRT-PCR data indicate biphasic metabolic differences between elementary bodies and reticulate bodies during infection. *Front Microbiol* 10:2350. <https://doi.org/10.3389/fmicb.2019.02350>.
  57. Sharick JT, Favreau PF, Gillette AA, Sdao SM, Merrins MJ, Skala MC. 2018. Protein-bound NAD(P)H lifetime is sensitive to multiple fates of glucose carbon. *Sci Rep* 8:5456. <https://doi.org/10.1038/s41598-018-23691-x>.
  58. Lakowicz JR, Szmacinski H, Nowaczyk K, Johnson ML. 1992. Fluorescence lifetime imaging of free and protein-bound NADH. *Proc Natl Acad Sci U S A* 89:1271–1275. <https://doi.org/10.1073/pnas.89.4.1271>.
  59. Chiarelli TJ, Grieshaber NA, Omsland A, Remien CH, Grieshaber SS. 2020. Single-inclusion kinetics of *Chlamydia trachomatis* development. *mSystems* 5:e00689-20. <https://doi.org/10.1128/mSystems.00689-20>.
  60. Schep DG, Zhao J, Rubinstein JL. 2016. Models for the a subunits of the *Thermus thermophilus* V/A-ATPase and *Saccharomyces cerevisiae* V-ATPase enzymes by cryo-EM and evolutionary covariance. *Proc Natl Acad Sci U S A* 113:3245–3250. <https://doi.org/10.1073/pnas.1521990113>.
  61. Patra KC, Hay N. 2014. The pentose phosphate pathway and cancer. *Trends Biochem Sci* 39:347–354. <https://doi.org/10.1016/j.tibs.2014.06.005>.
  62. Fendt S-M, Bell EL, Keibler MA, Olenchock BA, Mayers JR, Wasylenko TM, Vokes NI, Guarente L, Vander Heiden MG, Stephanopoulos G. 2013. Reductive glutamine metabolism is a function of the  $\alpha$ -ketoglutarate to citrate ratio in cells. *Nat Commun* 4:2236. <https://doi.org/10.1038/ncomms3236>.
  63. McCoy AJ, Adams NE, Hudson AO, Gilvarg C, Leustek T, Maurelli AT. 2006.  $\epsilon$ -L-Diaminopimelate aminotransferase, a trans-kingdom enzyme shared by *Chlamydia* and plants for synthesis of diaminopimelate/lysine. *Proc Natl Acad Sci U S A* 103:17909–17914. <https://doi.org/10.1073/pnas.0608643103>.
  64. Yang C, Kari L, Lei L, Carlson JH, Ma L, Couch CE, Whitmire WM, Bock K, Moore I, Bonner C, McClarty G, Caldwell HD. 2020. *Chlamydia trachomatis* plasmid gene protein 3 is essential for the establishment of persistent infection and associated immunopathology. *mBio* 11:e01902-20. <https://doi.org/10.1128/mBio.01902-20>.
  65. Zhong G. 2017. Chlamydial plasmid-dependent pathogenicity. *Trends Microbiol* 25:141–152. <https://doi.org/10.1016/j.tim.2016.09.006>.
  66. Li Z, Chen D, Zhong Y, Wang S, Zhong G. 2008. The chlamydial plasmid-encoded protein pgp3 is secreted into the cytosol of *Chlamydia*-infected cells. *Infect Immun* 76:3415–3428. <https://doi.org/10.1128/IAI.01377-07>.
  67. Liu Y, Huang Y, Yang Z, Sun Y, Gong S, Hou S, Chen C, Li Z, Liu Q, Wu Y, Baseman J, Zhong G. 2014. Plasmid-encoded Pgp3 is a major virulence factor for *Chlamydia muridarum* to induce hydrosalpinx in mice. *Infect Immun* 82:5327–5335. <https://doi.org/10.1128/IAI.02576-14>.
  68. Tiziani S, Lodi A, Khanim FL, Viant MR, Bunce CM, Günther UL. 2009. Metabolomic profiling of drug responses in acute myeloid leukaemia cell lines. *PLoS One* 4:e4251. <https://doi.org/10.1371/journal.pone.0004251>.
  69. Günther UL, Ludwig C, Rüterjans H. 2000. NMRLAB—advanced NMR data processing in matlab. *J Magn Reson* 145:201–208. <https://doi.org/10.1006/jmre.2000.2071>.
  70. Ludwig C, Günther UL. 2011. MetaboLab—advanced NMR data processing and analysis for metabolomics. *BMC Bioinformatics* 12:366. <https://doi.org/10.1186/1471-2105-12-366>.
  71. Love MI, Huber W, Anders S. 2014. Moderated estimation of fold change and dispersion for RNA-seq data with DESeq2. *Genome Biol* 15:550. <https://doi.org/10.1186/s13059-014-0550-8>.
  72. Liao Y, Smyth GK, Shi W. 2014. featureCounts: an efficient general purpose program for assigning sequence reads to genomic features. *Bioinformatics* 30:923–930. <https://doi.org/10.1093/bioinformatics/btt656>.